Precisely manipulating the local coordination of cobalt single-atom catalyst boosts selective hydrogenation of nitroarenes

Fengliang Cao [a,b], Wanxin Ni [a,c], Qingshan Zhao [a,*], Libo Wang [a], Song Xue [b], Yanpeng Li [a,b], Debin Kong [b,*], Mingbo Wu [b], Linjie Zhi [b,*]

[a] State Key Laboratory of Heavy Oil Processing, College of Chemistry and Chemical Engineering, China University of Petroleum (East China), Qingdao 266580, PR China
[b] College of New Energy, Advanced Chemical Engineering and Energy Materials Research Center, China University of Petroleum (East China), Qingdao 266580, PR China
[c] State Nuclear Power Demonstration Plant Co. Ltd, Rongcheng 264300, PR China

ARTICLE INFO

ABSTRACT

Manipulating the local coordination environment holds immense potential in augmenting the catalytic performance of single-atom catalysts, which remains a great challenge. Through theoretical prediction, we find the catalytic properties of atomic Co centers towards selective hydrogenation of nitroarenes can be effectively manipulated by adjusting the coordinated number of P atoms, among which Co-N$_2$P$_2$ configuration stands out. Accordingly, a single-atom Co$_1$-N/P-C catalyst featuring Co-N$_2$P$_2$ coordination was precisely fabricated through a sacrificial P-doped g-C$_3$N$_4$-template strategy. The optimal electronic structure of Co-N$_2$P$_2$ enables favorable chemical affinities toward nitroarene and H$_2$, promoted heterolytic dissociation of H$_2$, and accelerated reaction kinetics. Consequently, the Co$_1$-N/P-C catalyst exhibits outstanding catalytic activity (overall TOF of 241.5 h^{-1}), selectivity (>99%), and exceptional stability towards the hydrogenation of various functionalized nitroarenes, far surpassing other coordination configurations and most reported non-precious metal catalysts. This work deepens our understanding of the relationship between coordination structure and catalytic performance, offering boosted single-atom catalysts for selective hydrogenation of nitroarenes.

1. Introduction

Functionalized aromatic amines serve as the fundamental building blocks of fine chemicals, which have immense utilization for the production of pharmaceuticals, dyes, pigments, and other chemicals [1–4]. Catalytic hydrogenation of nitroarenes has emerged as an environmentally benign and recyclable approach for synthesizing value-added amines [5–7]. Nevertheless, selective reduction of the −NO$_2$ moiety while reserving other reducible groups (e.g., halogens, alkenes, and ketones, etc.) is an immensely desirable yet challenging task [8–10]. In this regard, significant efforts have been devoted to harnessing efficient catalysts for the chemoselective hydrogenation of nitroarenes [11–13]. Despite the remarkable catalytic activities exhibited by precious metal catalysts, such as Au [14], Pt [15,16], Pd [17,18], etc., they generally suffer from high cost, unsatisfactory selectivity, and suboptimal atomic utilization. Thus, efficient, cost-effective, and highly selective catalysts for the hydrogenation of nitroarenes are still urgently needed [19].

It is worth mentioning that non-precious metal catalysts have been extensively studied as substitutes due to their affordability, economical nature, and excellent selectivity [20–22]. Among them, transition metal-nitrogen-carbon single-atom catalysts (M-N-C, M=Fe [23], Co [24,25], Ni [26], etc.), particularly Co-N-C single-atom catalysts, have displayed exceptional catalytic efficacy compared to their counterparts on account of the maximum atom efficiency, unique electronic structure, and tunable coordination environment. For instance, Bu et al. synthesized a series of single-atom catalysts with M-N$_4$ configuration through defect engineering of metal-organic frameworks (MOFs) [27]. The optimized Co SAs/NC-800 catalyst demonstrated high activity and stability for the selective hydrogenation of nitroarenes. Considering the reaction occurs at the gas-liquid-solid three-phase interface, the adsorption of nitroarenes and activation of hydrogen are the crucial steps that determine the catalytic performance [28]. However, the symmetrical electron distribution of typical Co-N$_4$ configuration limits the conversion due to the weak adsorption and/or excessive activation of the reactants [29,30]. Therefore, enhancing the activity while upholding the high selectivity of Co-N-C single-atom catalysts is an

essential precondition for further widespread applications.

In most cases, the central metal atoms of single-atom catalysts are firmly attached to the support material by coordination with four N atoms to construct M-N$_4$ configurations [31,32]. Most recently, many studies have been dedicated to incorporating non-nitrogen (O, P, S, etc.) atoms in order to improve the intrinsic activity of M-N$_4$ towards diverse chemical and electrochemical reactions [33]. Due to the different electronegativity and atomic radius with the N atom, the introduction of heteroatoms can effectively modulate the electronic and geometric structure of the central metal atoms, thereby influencing the adsorption behavior and catalytic performance [34–36]. For instance, Liu and co-workers reported a single-atom dispersed cobalt catalyst with Co$_1$-N$_3$S$_1$ active sites, which showed excellent catalytic performance for the hydrogenation of N-heterocycles [37]. Representatively, Cao et al. introduced P heteroatom as electron donors to fabricate a single-atom Co$_1$/NPC catalyst featuring Co-N$_3$P$_1$ centers, which achieved unprecedentedly enhanced activity and chemoselectivity for the hydrogenation of functionalized nitroarenes compared to the Co-N$_4$ coordination [38]. Despite these achievements, the impact of heteroatom quantity on the electronic structure of metal centers and catalytic properties remains ambiguous. Therefore, it is desirable to precisely manipulate the local coordination environment of metal single-atom sites and unravel the structure-activity correlation in the pursuit of advanced catalysts.

Considering the effectivity of reinforcing the intrinsic activity through P doping, we first performed theoretical calculations to predict the nitroarene hydrogenation over a series of atomic Co-N$_x$P$_{(4-x)}$ configurations with varying P coordination atoms. According to the calculation results, Co-N$_2$P$_2$ emerges as an intriguing candidate for promoting the adsorption of nitroarene substrate and activating molecular hydrogen, thus reinforcing the selective hydrogenation of nitroarenes. Inspired by the theoretical predictions, we rationally designed a sacrificial P-doped g-C$_3$N$_4$-template strategy to construct an atomically dispersed Co catalyst (Co$_1$-N/P-C) with the desired Co-N$_2$P$_2$ configuration. Owing to the optimal electronic structure of Co-N$_2$P$_2$, the Co$_1$-N/P-C catalyst exhibits significantly boosted catalytic activity (overall TOF = 241.5 h^{-1}) and selectivity (>99%) toward the hydrogenation of *p*-chloronitrobenzene, as well as a series of substituted nitroarenes with the co-existence of sensitive reducible groups, outperforming other Co-N$_x$P$_{(4-x)}$ configurations and most reported non-precious metal catalysts. Furthermore, the correlation between coordination structure and catalytic performance is unveiled, shedding light on the catalytic nature of the single-atom catalysts.

2. Experimental

2.1. Materials and chemicals

Petroleum pitch was acquired from China National Oil Corporation (19.63 wt% saturates, 35.76 wt% aromatics, 37.21 wt% resins, and 7.40 wt% asphaltenes). Melamine (99 wt%), ammonium chloride (NH$_4$Cl, 99.8 wt%), triammonium phosphate trihydrate ((NH$_4$)$_3$PO$_4$•3H$_2$O, 98 wt%), ethanol (99.5%), hydrogen chloride (HCl, 37 wt%), cobalt chloride hexahydrate (CoCl$_2$•6H$_2$O, 99 wt%), ethanol (99 wt%), toluene (99 wt%), sodium borohydride (NaBH$_4$, 98 wt%), potassium thiocyanate (KSCN, 99 wt%), dodecane (99.5 wt%), p-nitrochlorobenzene (*p*-CNB, 98 wt%), p-nitrofluorobenzene (98 wt%), p-nitrobromobenzene (99 wt%), p-nitroiodobenzene (99 wt%), p-nitrophenol (98 wt%), nitrobenzene (99 wt%), p-nitrotoluene (99 wt%), p-nitrobenzonitrile (97 wt%), p-nitrobenzyl alcohol (98 wt%), and p-nitrostyrolene (99 wt%) were purchased from Aladdin Industrial Corporation. All the chemical reagents were used as received without any further purification.

2.2. Synthesis of P-doped graphitic carbon nitride (P-eg-C$_3$N$_4$)

5 g of melamine, 2.5 g of NH$_4$Cl, and 0.3 g of (NH$_4$)$_3$PO$_4$•3 H$_2$O were thoroughly ground into a homogeneous power, which was then heated from room temperature to 520 °C at a rate of 2.3 °C min^{-1} under air atmosphere and kept for 4 h. Afterwards, the product was washed with deionized water for several times, and the P-doped graphitic carbon nitride was obtained, labeled as P-eg-C$_3$N$_4$. Additionally, P-eg-C$_3$N$_4$-1 and P-eg-C$_3$N$_4$-3 templates were prepared by varying the amount of (NH$_4$)$_3$PO$_4$•3 H$_2$O to 0.15 g and 0.45 g, respectively. As controls, bulk carbon nitride (b-C$_3$N$_4$) was prepared by the same procedure except for the addition of NH$_4$Cl and (NH$_4$)$_3$PO$_4$•3 H$_2$O. Exfoliated carbon nitride (eg-C$_3$N$_4$) was prepared without the addition of (NH$_4$)$_3$PO$_4$•3H$_2$O.

2.3. Synthesis of Co$_1$-N/P-C catalyst

The prepared P-eg-C$_3$N$_4$ precursor was dispersed into ethanol by ultrasonication for 0.5 h. Subsequently, CoCl$_2$•6H$_2$O was added into the solution of P-eg-C$_3$N$_4$, and the chelating process between P-eg-C$_3$N$_4$ and Co^{2+} took place at 25 °C for 8 h with magnetic stirring. The resulting product, where Co^{2+} was firmly anchored onto P-eg-C$_3$N$_4$ (designated as Co^{2+}-P-eg-C$_3$N$_4$), was collected by filtration and washed thoroughly with deionized water to remove the excessive Co^{2+}. Furthermore, 1 g of Co^{2+}-P-eg-C$_3$N$_4$ powder and 0.25 g of petroleum asphalt were dispersed in a toluene solution and subjected to ultrasonication for 0.5 h. The mixture was subsequently dried through distillation under reduced pressure to obtain a gray power, which was carbonized at 900 °C for 2 h with a heating rate of 5 °C min^{-1} under N$_2$ atmosphere. The power was etched in a 1 M HCl solution for 24 h to obtain the Co$_1$-N/P-C catalyst. In addition, Co$_1$-N-C was synthesized using the same method by replacing P-eg-C$_3$N$_4$ with eg-C$_3$N$_4$. Co$_1$-N/P-C-1 and Co$_1$-N/P-C-3 were prepared by using P-eg-C$_3$N$_4$-1 and P-eg-C$_3$N$_4$-3 as the template. As a control, petroleum asphalt-derived carbon (PAC) was directly prepared by calcining petroleum asphalt at 900 °C under the N$_2$ atmosphere.

2.4. Characterization

Power X-ray diffraction (XRD, X′Pert PRO MPD) equipped with Cu Kα radiation (k = 1.518 Å) was used to analyze the crystal structure of the samples. *In-situ* Fourier-transform infrared spectroscopy (FTIR, Thermo NEXUS 470) experiments were conducted based on the transmissive mode to investigate the chemisorption of reactants on the catalysts. The microstructure and morphology were characterized by Scanning electron microscopy (SEM, Hitachi S-4800) and transmission electron microscopy images (TEM, FEI-Talos F200X). Aberration-corrected scanning transmission electron microscopy (AC-STEM) images were carried out on an FEI-Titan Cubed Themis G2 300 operated at 300 kV. The specific surface area was calculated by the Brunauer-Emmett-Teller (BET) method based on a Micromeritics ASAP 2020 instrument. X-ray photoelectron spectroscopy (XPS) spectra were performed by a monochromatic Mg Kα radiation (1486.6 eV) X-ray source (Thermo Scientific Escalab 250XI). The metal content was detected by inductively coupled plasma-optical emission spectrometer (ICP-OES, Vista-MPX). X-ray absorption near edge structure (XANES) and extended X-ray absorption fine structure (EXAFS) were performed at 1W1B station in Beijing Synchrotron Radiation Facility (BSRF). The hydrogen temperature-programmed desorption (H$_2$-TPD) was conducted on a PCA-1200 apparatus equipped with a thermal conductivity detector. The catalytic performance of the catalysts was determined by gas chromatography (GC, BF-2022) with a flame-ionization detector.

2.5. Adsorption experiment

The adsorption amounts of *p*-CNB on Co$_1$-N-C and Co$_1$-N/P-C were measured by adding the sample (10 mg) into 10 mL of ethanol containing 20 µmol of the adsorbate. The suspension was stirred continuously at room temperature for 4 h and then left to stand for 8 h. The solid catalyst was separated from the reaction system by centrifugation. Then the concentration of the remaining adsorbate was measured with ultraviolet–visible (UV–vis) spectroscopy. The adsorption capacity can

be calculated as follows: Adsorption capacity = [Total amount of *p*-CNB - residual amount of *p*-CNB (μmol)] / [catalyst weight (g)].

2.6. Catalytic hydrogenation of nitroarenes

An autoclave (50 mL) was filled with the following ingredients for the typical hydrogenation of nitroarenes procedure: substrates (0.5 mmol), catalyst (10 mg), internal standard (dodecane, 0.5 mmol), and solvent (ethanol, 10 mL). The autoclave was charged with 2 MPa H_2 after being purged with N_2 and H_2 three times. Then, the reaction was carried out at 100 °C for 2 h with magnetic stirring of 800 rpm. After the reaction, the suspension was filtrated and analyzed using a GC equipped with a DB-WAXetr analytical column. For the recycling tests, the catalyst was collected via filtration and dried under a vacuum, which was reused in subsequent cycles. The overall turnover frequency (TOF) was calculated as: TOF (h^{-1}) = [mol of substrate reduced] / [mol of metallic Co * reaction time (h)].

2.7. Density functional theory (DFT) calculations

DFT calculations were performed using Ab-initio Simulation Package (VASP 5.4.1). All electron exchange-correlation functionals were calculated using the generalized gradient approximation (GCA) with the revised Perdew-Burke-Ernzerhof (PBE) method using a cutoff energy of 500 eV. Based on the lattice size, the Monkhorst-Pack meshes of 3 × 3 × 1 k-point samplings in the surface Brillouin zones were used for the graphene surfaces with a unit cell of 5 × 5 × 1. A vacuum layer exceeding 15 Å was used to avoid periodic interactions. The atomic position was fully relaxed until the maximum force on each atom was

less than − 0.01 eV/ Å and 10^{-5} eV. The selection of these parameters was based on convergence tests with respect to the total energy of the systems. The barriers for H_2 decomposition over Co-N_4 and Co-N_2P_2 configuration were determined using the climbing-image nudged elastic band (CI-NEB) approach.

3. Results and discussion

3.1. Theoretical prediction of nitroarene hydrogenation on Co-$N_xP_{(4-x)}$

To unravel the impact of P doping on the electronic structure of the Co center and predict corresponding catalytic properties towards the selective hydrogenation of nitroarenes, we built a series of Co-$N_xP_{(4-x)}$ (x = 0, 1, 2, 3, and 4) models with alterable P coordination atoms and conducted density functional theory (DFT) calculations (Fig. S1). Bader charge transfer (Fig. 1a) and charge density difference (Fig. 1b) were firstly explored to examine the influence of P-atom number on the electron density of central Co. Compared with the pristine Co-N_4 configuration, it is evident that the insertion of P atoms induces significant alterations in the Bader charge transfer number and charge density difference between the Co center and the ligands. The electron density in the Co-3d orbitals increases with the increasing number of coordinated P atoms, turning from positive to negative charge due to the weaker electronegativity of P (2.19) compared to N (3.04) [39]. Such electron redistribution is anticipated to motivate distinct interactive behaviors with the nitroarene and H_2 substrates. The projected density of states (PDOS) of the Co-3d orbitals in Co-$N_xP_{(4-x)}$ were calculated and described by the values of the d-band center location relative to the Fermi level. As depicted in Fig. 1c and Fig. S2, the d-band center shifts of
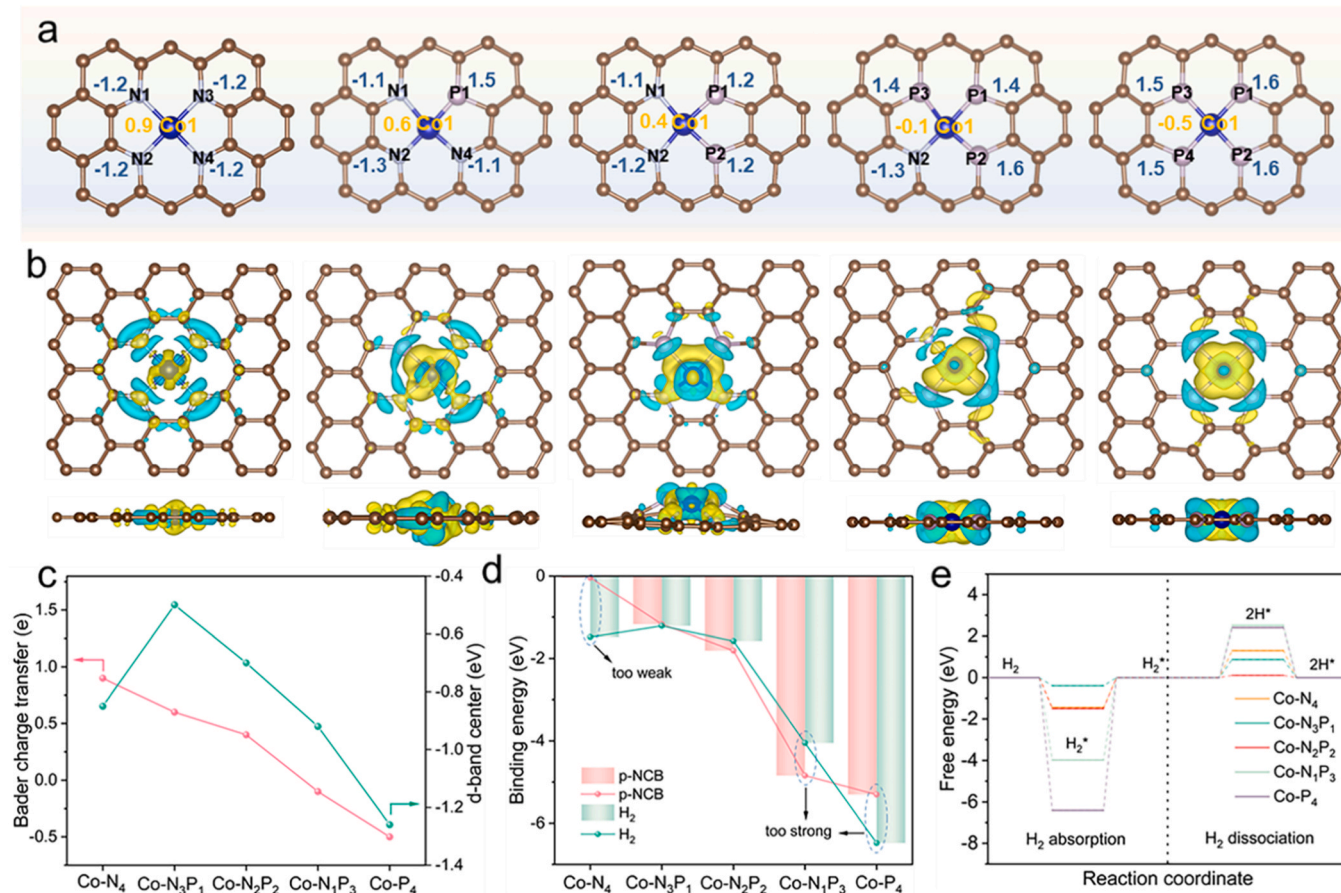

Fig. 1. (a) Bader charge transfer numbers and (b) charge density difference of the coordination atoms of Co-$N_xP_{(4-x)}$. Yellow and blue represent electron gain and loss, respectively. (c) Bader charge transfer numbers and d-band center of Co in Co-$N_xP_{(4-x)}$. (d) Binding energy of *p*-CNB and H_2 on the surface of Co-$N_xP_{(4-x)}$. (e) Calculated free energy diagram for H_2 adsorption and dissociation.

Co-N$_2$P$_2$ and Co-N$_3$P$_1$ are much smaller than those of the other three configurations, potentially contributing to strengthened catalytic activity according to the d-band center theory [40].

To shed further light on the influence of coordination structure on the catalytic characteristics, the crucial steps for nitroarene hydrogenation involving the adsorption of the reactants and H$_2$ dissociation were studied. As shown in Fig. 1d, the regular Co-N$_4$ configuration shows feeble interaction with *p*-CNB, while the binding energy increases as the electron density in Co-3d orbitals rises (Fig. 1d). This result is in good accordance with the Bader charge transfer between the Co center and *p*-CNB (Fig. S3), indicating that the introduction of variable P atoms effectively affects the adsorption behavior. Following the Sabatier principle, excessively strong interaction between the Co center and *p*-CNB would passivate the catalytic sites due to severe obstruction of the reaction [41]. Accordingly, the Co-N$_2$P$_2$ and Co-N$_3$P$_1$ configurations would offer favorable interactions with *p*-CNB and facilitate the subsequent transformations. With regard to H$_2$ adsorption, the binding energy initially decreases from Co-N$_4$ to Co-N$_3$P$_1$ but then increases with the further insertion of coordinated P atoms. Notably, Co-N$_2$P$_2$ manifests a moderate interaction with H$_2$ and displays the lowest energy barrier for H$_2$ dissociation, suggesting the reinforced charge resonance capability of Co-N$_2$P$_2$ in expediting the H$_2$ dissociation process (Fig. 1e). Consequently, breaking the symmetric charge distribution of Co-N$_4$ through the introduction of P atoms contributes to heightened electronic localization and spin polarization, which would significantly affect the adsorption and catalytic behaviors [42]. Among the various Co-N$_x$P$_{(4-x)}$ configurations, the Co-N$_2$P$_2$ with an optimal electronic structure emerges as an intriguing candidate for promoting the adsorption of nitroarene substrate and activating the molecular hydrogen, thus effectively reinforcing the selective hydrogenation of nitroarenes.

3.2. Synthesis and characterization of Co-based single-atom catalysts

Based on the theoretical discoveries, we sought to construct an atomically dispersed Co catalyst with the desired Co-N$_2$P$_2$ configuration. Owing to the high nitrogen content (57.1 at%), cost-effectiveness, and environment-friendly nature, graphitic carbon nitride (g-C$_3$N$_4$) serves as an ideal template and precursor, which allows for the firmly anchoring of single metal atoms within the six-fold coordination sites formed by neighboring nitride groups [43]. Considering the limited specific surface area of traditional g-C$_3$N$_4$ and the absence of P atoms, NH$_4$Cl and (NH$_4$)$_3$PO$_4$ were introduced as additional gaseous precursors to engineer porous and P-doped g-C$_3$N$_4$ (P-eg-C$_3$N$_4$) with a high-porosity lamellar structure (Fig. S4), which shows a surface area of 42.0 m^2/g, 4.4 times higher than that of b-C$_3$N$_4$ (9.6 cm^2/g). During the thermal polymerization process, NH$_4$Cl and (NH$_4$)$_3$PO$_4$ decomposed into gaseous NH$_3$, HCl, and H$_3$PO$_4$ species, leading to the exfoliation of b-C$_3$N$_4$ into ultrathin nanosheets (Fig. S5). Simultaneously, the resulting H$_3$PO$_4$ incorporated P atoms into the framework of g-C$_3$N$_4$ via polymerization (Fig. S6). DFT calculations reveal that the pre-intercalation of P atoms into the g-C$_3$N$_4$ framework is beneficial to the formation of atomically dispersed Co sites with Co-P coordination (Fig. S7). To engineer the targeted Co-N$_2$P$_2$ configuration, the local coordination environment of Co-N$_x$ was precisely manipulated by controlling the amount of (NH$_4$)$_3$PO$_4$. Fourier-transform infrared (FT-IR) spectra (Fig. S8a) and X-ray diffraction (XRD) patterns (Fig. S8b) confirm that the exfoliation and P-doping processes do not irreversibly damage the framework structure of g-C$_3$N$_4$. After anchoring the Co^{2+} precursor onto the
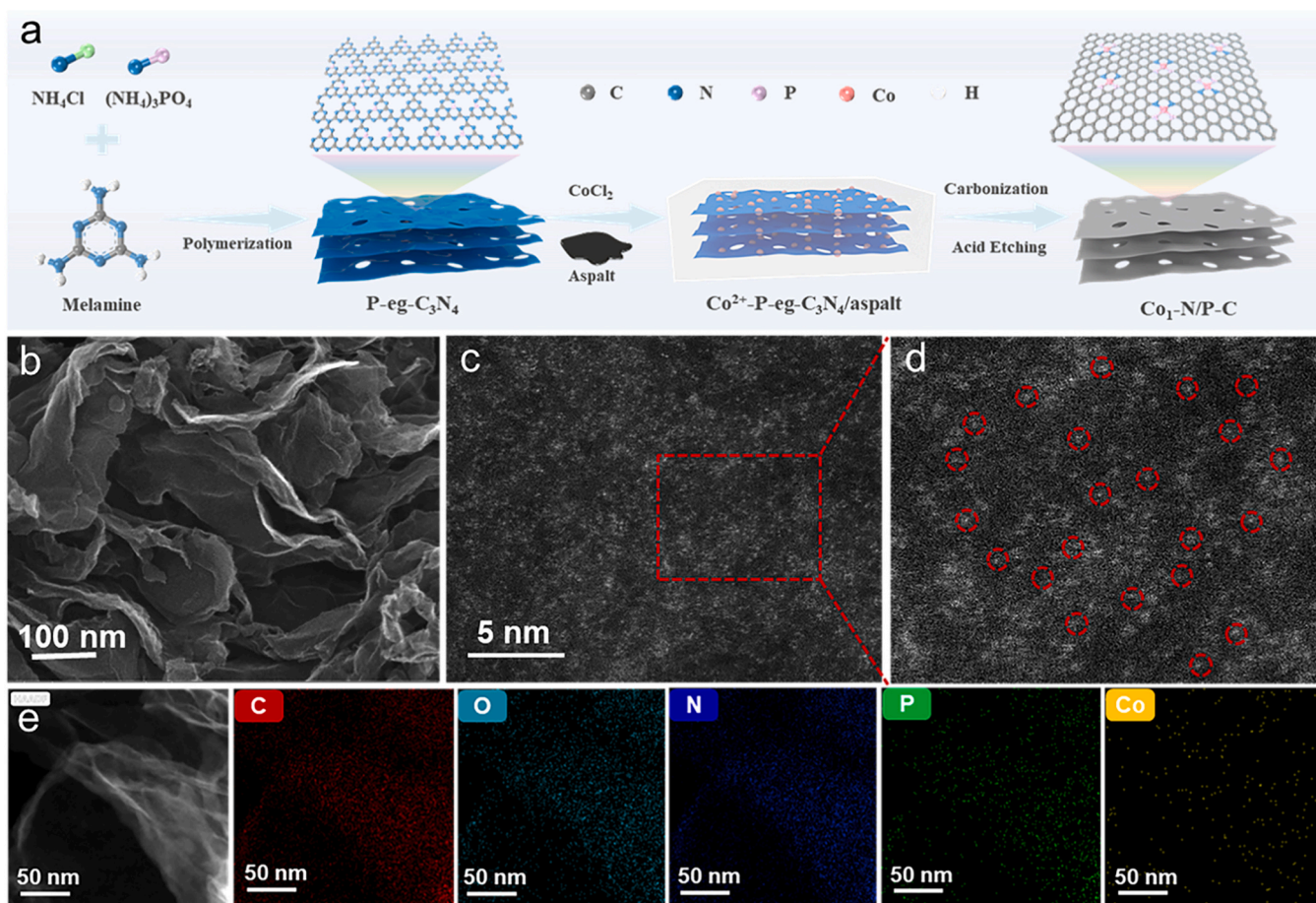

Fig. 2. (a) Schematic illustration for the preparation procedure of Co$_1$-N/P-C. (b) SEM image of Co$_1$-N/P-C. (c, d) AC-STEM image of Co$_1$-N/P-C. (e) TEM image and corresponding element mapping of Co$_1$-N/P-C.

P-eg-C_3N_4 matrix, the resulting Co^{2+}-P-eg-C_3N_4 intermediate was coated with highly viscous petroleum pitch, which provides a versatile carbon source that suppressed metal migration and agglomeration during the subsequent carbonization process [44,45]. Thus, the single-atom Co_1-N/P-C catalyst was rationally designed and fabricated through the sacrificial P-doped g-C_3N_4-template strategy (Fig. 2a), and a series of Co-based catalysts were fabricated by introducing a varying amount of P-dopant. The Co_1-N-C single-atom catalyst without P doping was synthesized by replacing P-eg-C_3N_4 with eg-C_3N_4.

The microstructure and morphology of Co_1-N-C and Co_1-N/P-C were characterized by Scanning electron microscopy (SEM) and transmission electron microscopy (TEM). As shown in Fig. 2b and Fig. S9-10, the Co_1-N-C and Co_1-N/P-C consist of an abundance of graphene-like nanosheets derived from the layered template of P-eg-C_3N_4. Notably, no discernible metal nanoparticles can be observed, as further evidenced by the XRD results that exclusively exhibit the characteristic peaks of amorphous graphite at 43° and 26° for Co_1-N/P-C and Co_1-N-C (Fig. S11). These results unveil the template role of eg-C_3N_4 and P-eg-C_3N_4, as well as the absence of agglomerated metallic phases in Co_1-N/P-C and Co_1-N-C. Furthermore, aberration-corrected scanning TEM (AC-STEM) was employed to elucidate the existence of Co species. Abundant isolated bright spots corresponding to Co can be observed on the carbon substrate, indicating the formation of the atomically dispersed Co atoms in Co_1-N/P-C (Fig. 2c-d) and Co_1-N-C (Fig. S12). By reducing the amount of

$(NH_4)_3PO_4$ precursor, a Co_1-N/P-C-1 catalyst with atomically dispersed Co atoms was also obtained (Fig. S13). Whereas the P-eg-C_3N_4-3 template results in a large number of metal nanoparticles coated with a carbon layer distributed on the skeleton of Co_1-N/P-C-3, revealing the severe metal aggregation with increased P dopant under the pyrolysis condition. Energy-dispersive X-ray spectroscopy (EDS) mappings of Co_1-N/P-C and Co_1-N-C further demonstrate the uniform dispersion of all elements throughout the entire structure (Fig. 2e and Fig. S14). According to the inductively coupled plasma optical emission spectrometry (ICP-OES) analysis, the Co contents in Co_1-N/P-C and Co_1-N-C are determined to be 0.61 and 0.70 wt%, respectively (Table S1). The observations in Raman spectra (Fig. S15), wherein the I_D/I_G values of Co_1-N-C (1.04) and Co_1-N/P-C (1.03) are higher than that of APC (0.96), suggest an increase in carbon disorder due to the introduction of Co, N, and P dopants. To reveal the pore structure and specific surface areas, N_2 adsorption/desorption isotherms were collected. Co_1-N/P-C and Co_1-N-C both exhibit type-IV isotherms with H3 hysteresis loops, indicating a porous lamellar structure (Fig. S16a) [46]. The specific surface areas of the two samples are measured to be 250.3 and 646.3 m^2 g^{-1}, respectively. The significantly reduced surface area of Co_1-N/P-C should be ascribed to its ultrathin layer structure after P doping (Fig. S5). Corresponding pore size distribution results reveal the presence of abundant micropores in the samples arising from the pore-forming effect from g-C_3N_4 template decomposition (Fig. S16b) [47]. Such abundant
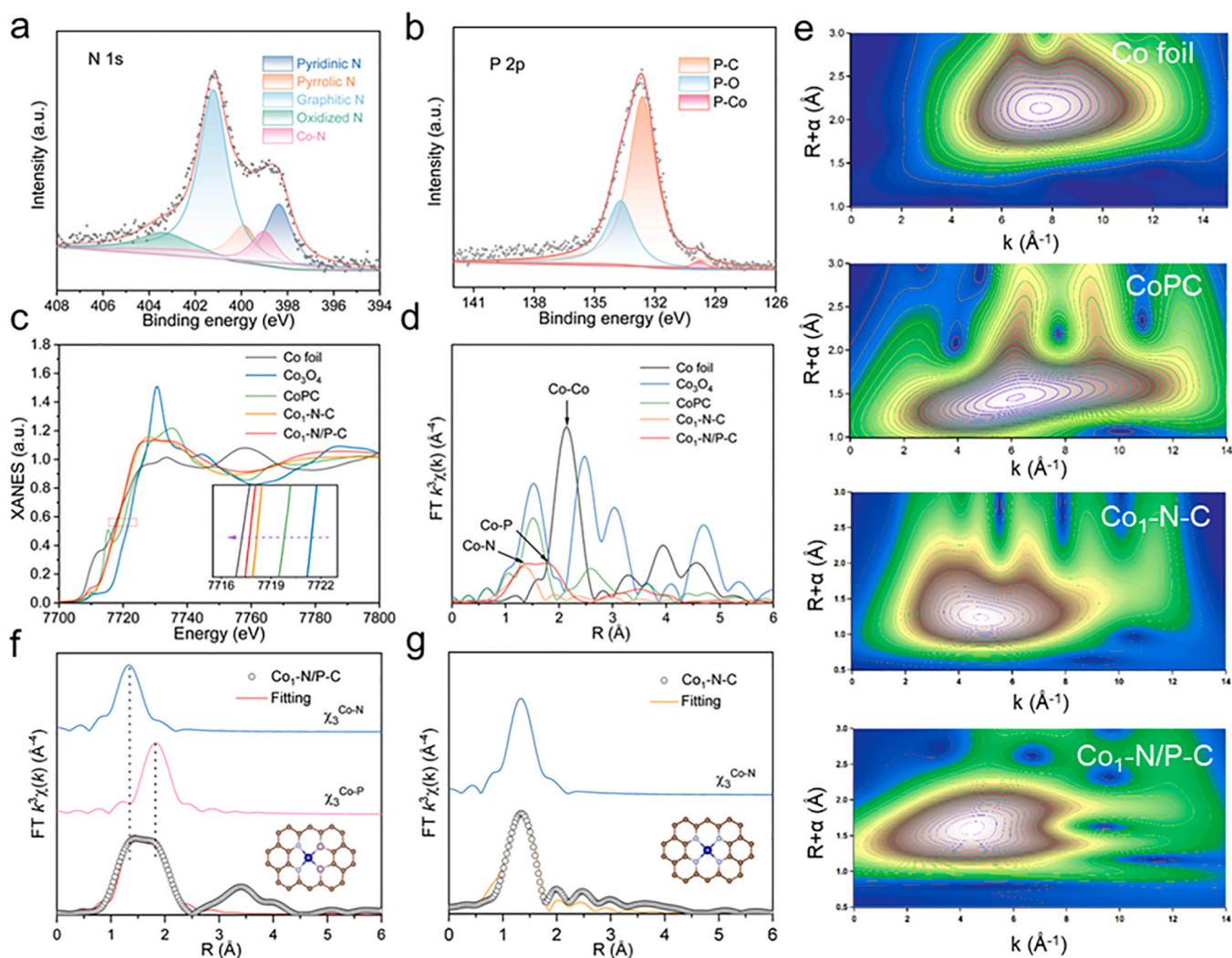

Fig. 3. (a) N 1 s and (b) P 2p high-resolution XPS spectra of Co_1-N/P-C. (c) XANES and (d) FT-EXAFS spectra of Co_1-N/P-C and the references. (e) WT Co K-edge EXAFS profiles of Co foil, CoPC, Co_1-N-C, and Co_1-N/P-C. (f) EXAFS fitting curves of Co_1-N/P-C in the R space. (g) EXAFS fitting curves of Co_1-N-C in the R space.

micropores and lamellar structures would provide accessible pathways for the rapid transport and adsorption of reactants to the atomic metal sites in subsequent reaction processes.

The element chemical states in the two Co-based single-atom catalysts were further investigated by X-ray photoelectron spectroscopy (XPS). The XPS survey spectrum of Co_1-N-C reveals the presence of C, N, O, and Co signals, with an additional P signal in Co_1-N/P-C, implying the successful ternary (Co/N/P) doping of Co_1-N/P-C (Fig. S17-18). The quantification analysis of the elemental composition is listed in Table S1. The high-resolution N 1 s spectrum of Co_1-N/P-C can be deconvoluted into five types of N species located at 398.2 (pyridinic N), 399.2 (Co-N), 400.0 (pyrrolic N), 401.1 (graphitic N), and 403.5 eV (oxidized N), respectively (Fig. 3a) [38]. Similar peaks can be observed for the Co_1-N-C catalyst shown in Fig. S17. Remarkably, as illustrated in Fig. 3b the high-resolution P 2p spectrum exhibits a characteristic peak at approximately 129. 5 eV corresponding to the Co-P bond in Co_1-N/P-C, which is absent in the Co_1-N-C sample. These results indicate that the atomically dispersed Co atoms display dual-coordinated configurations of Co-N and Co-P in Co_1-N/P-C, whereas only Co-N coordinated configuration is present in Co_1-N-C.

X-ray absorption fine spectroscopy (XAFS) measurements were conducted to unravel the coordination environment of Co atoms. Fig. 3c presents the X-ray near-edge structures (XANES) spectra of Co_1-N/P-C and Co_1-N-C, with Co foil, Co_3O_4, and cobalt phthalocyanine (CoPC) serving as reference samples. The adsorption edge position for Co in Co_1-N/P-C is located between Co foil and CoPC, suggesting a valence state ranging from 0 to + 2 [48]. Compared to Co_1-N-C, Co_1-N/P-C displays a lower pre-edge absorption energy, indicating the lower oxidation state of Co. According to the aforementioned Bader charge transfer analysis in Fig. 1a, the weaker electronegativity of P makes it an electron donor to efficiently modulate the electron density of the metal centers. The k^3-weighted Fourier transforms EXAFS spectrum of Co_1-N/P-C displays a relatively broad peak at around 1.5 Å, indicating the coexistence of Co-N (1.35 Å) and Co-P (1.75 Å) coordination (Fig. 3d). Notably, the Co-Co peak at 2.2 Å is neglectable, indicating that the Co atoms are dispersed at the atomic level. To further examine the atomic dispersion of Co in the samples, wavelet transform (WT) of Co K-edge EXAFS (WT-EXAFS) was performed (Fig. 3e). In contrast to the WT plots of Co foil and CoPC, Co_1-N/P-C, and Co_1-N-C only show one intensity maximum at around 4.5 $Å^{-1}$, with no corresponding intensity maximum for Co-Co. Quantitative least-squares EXAFS curve fitting analysis was performed to extract the coordination configuration around the atomic Co sites. In comparison, the fitting results for Co foil and CoPC are depicted in Fig. S19. As shown in Fig. 3f-g and fitting parameters listed in Table S2, the Co atom in Co_1-N/P-C is coordinated by two N atoms at 1.95 Å and two P atoms at 2.28 Å, revealing the precise construction of Co-N_2P_2 configuration. Notably, the fitting results confirm Co-N_4 and Co-N_3P_1 configurations for Co_1-N-C and Co_1-N/P-C-1, respectively. Co_1-N/P-C-3 shows an increased coordination number of Co-P (3.3) than that of Co_1-N/P-C, as well as the presence of the Co-Co bond (Fig. S20). Combined with the above TEM images, this result reveals the generation of abundant CoP_x and Co(0) species with the presence of excessive phosphorus precursor, rather than Co-N_1P_3 or Co-P_4 moieties. This is supported by the high positive formation energies of Co-N_1P_3 and Co-P_4 configurations (Fig. S21). According to the coordination numbers in Table S2, atomic Co-N_2P_2, CoP_x, and metallic Co are presumed to be the active species in the Co_1-N/P-C-3 catalyst. Based on these findings, we demonstrate the engineering of a Co_1-N/P-C single-atom catalyst featuring the favorable Co-N_2P_2 configuration through a sacrificial P-doped g-C_3N_4-template strategy. Besides, a series of Co-based catalysts with diverse coordination configurations were simultaneously prepared to reveal the coordination structure-performance correlation.

3.3. Catalytic hydrogenation of nitroarenes

To evaluate the catalytic performance of the prepared Co-based

single-atom catalysts, the selective hydrogenation of p-chloronitrobenzene (p-CNB) to p-chloroaniline was first conducted at 100 °C in the presence of H_2 (2 MPa) for 2 h. As depicted in Fig. 4a, the metal-free N/P-C support exhibits a poor conversion of less than 10%. The Co_1-N-C catalyst with traditional Co-N_4 configuration displays an inferior yield of 14% under identical reaction conditions, indicating its limited ability to adsorb and activate the reactants (Table S4). In comparison, Co_1-N/P-C-1 shows an enhanced catalytic activity and achieves a conversion of 35% with a high selectivity of 99%, implying the effectiveness of P doping. To our delight, the implementation of Co_1-N/P-C results in a remarkable increase in both conversion (>99%) and selectivity (>99%), highlighting the exceptional catalytic performance of the Co-N_2P_2 active sites. A dramatic decrease in catalytic activity (42%) can be observed on Co_1-N/P-C-3, which should be attributed to the presence of CoP_x and metallic Co species apart from atomic Co-N_2P_2. Further carbon balance results reveal the efficient conversion of p-CNB to p-chloroaniline over the Co-based catalysts without over-hydrogenation or generating other gaseous products (Table S5). As controls, commercial Pt/C (Fig. 4a) and Pd/C (Table S4) catalysts both give commendable catalytic activities but terrible selectivity due to simultaneous dehalogenation, even under atmospheric H_2 pressure. The catalytic results elucidate the correlation between coordination structure and catalytic performance, in good agreement with the above theoretical predictions. To identify the intrinsic active centers of Co_1-N/P-C, thiocyanate ion (SCN^-) poisoning experiments were conducted. Atomic Co sites can be poisoned and deactivated by SCN^-, while nanoparticles would remain unaffected (Fig. 4b). After being treated with KSCN for 12 h, the conversion of Co_1-N/P-C witnesses a significant decline from over 99% to 10.7%, comparable to the metal-free N/P-C. These results validate the dominating contribution of atomically dispersed Co-N_2P_2 sites for the reaction. In addition, the Co_1-N/P-C catalyst exhibits superior stability and reusability, as demonstrated by negligible deterioration in catalytic activity and selectivity after 10 consecutive cycles (Fig. 4c). The excellent stability of the Co_1-N/P-C catalyst was further confirmed by hot-filtration experiments (Fig. S22). The solid catalyst was separated from the reaction system by filtration after reaction for 1 h. Despite extending the reaction time to 3 h under the same conditions, no further increase in conversion is observed. This substantiates that no cobalt species leaches into the solvent, contributing to the remarkable stability of Co_1-N/P-C. In light of the versatile catalytic efficiencies, the overall turnover frequency (TOF) was calculated to compare its performance with the reported catalysts. The overall TOF of Co_1-N/P-C is determined to be 241.5 h^{-1}, 7.8 times higher than that of Co_1-N-C (30.8 h^{-1}). Remarkably, the catalytic performance of Co_1-N/P-C surpasses that of most reported non-precious metal catalysts (Fig. 4e and Table S6).

The solvent is one of the crucial factors that influence the activity and selectivity for selective hydrogenation of nitroarenes. Therefore, the reactions were further carried out in various solvents, including ethanol, ethanol/water, N, N-dimethylformamide (DMF), and toluene (Table S7). High conversions were obtained in protonated solvents (ethanol and ethanol/water), while p-CNB could not be efficiently converted to p-chloroaniline in non-protonated solvents (DMF and toluene), suggesting that the proton group in protic solvents play an important role in the catalytic hydrogenation process. Furthermore, apart from molecule hydrogen, a wide range of reductant and hydrogen sources was employed to examine the activation property of Co_1-N/P-C. As illustrated in Fig. 4d, Co_1-N/P-C exhibits impressive catalytic activity and selectivity by employing $NaBH_4$, $NH_3 \bullet BH_3$, and $N_2H_4 \cdot H_2O$ as the reductant, with overall TOF values of 14491.8, 181.1, and 120.8 h^{-1}, respectively. Additionally, selective hydrogenation of various substituted nitroarenes with varying functionalized groups was explored under identical reaction conditions (Table 1). Impressively, Co_1-N/P-C shows extraordinary chemoselectivity for the hydrogenation of various functionalized nitroarenes with other sensitive reducible groups, such as alkenyl (94%, 2a), halogen (>90%, 2b-e), nitrile groups (>99%, 2 f). In the case of substituted nitroarenes with electron-donating groups, an
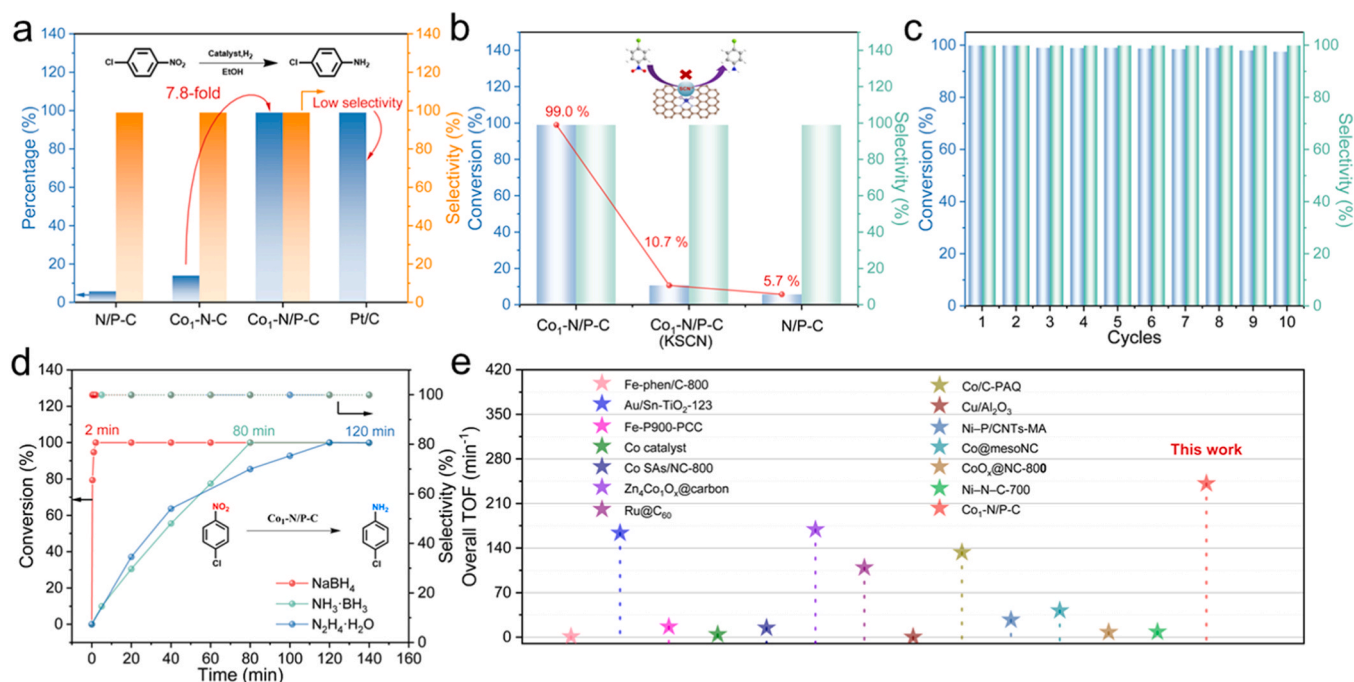
Fig. 4. (a) Catalytic performance of N/P-C, Co$_1$-N-C, Co$_1$-N/P-C, and Pt/C for *p*-CNB hydrogenation. (b) Poisoning test of Co$_1$-N/P-C. (c) Recyclability tests of Co$_1$-N/P-C. (d) Catalytic performance of *p*-NCB reduction over Co$_1$-N/P-C with different hydrogen-donor agents. Reaction conditions: [a] 0.1 mmol *p*-CNB, 20 mL water/ethanol (v/v=1:1), 12.5 equivalent of NaBH$_4$, 2 mg catalyst, 30 °C. [b] 0.5 mmol *p*-NCB, 10 mL of ethanol, 4.0 equivalent N$_2$H$_4$·H$_2$O or NH$_3$·BH$_3$, 60 °C. (e) Comparison of the catalytic performance with reported catalysts.

Table 1
Chemoselective hydrogenation of various nitroarenes over Co$_1$-N/P-C.

Standard reaction condition: 0.5 mmol nitroarene substrate in 10 mL ethanol, 10 mg catalyst, 100 °C, 2 MPa H$_2$.

almost impeccable 99% selectivity could be achieved. ^{1}H NMR tests of the reaction products further confirm the effective conversion of nitroarenes to corresponding amines over the Co-N$_2$P$_2$ active sites (Fig. S23). The outstanding activity and satisfactory selectivity should be attributed to the distinctive nature of asymmetrically coordinated Co-N$_2$P$_2$ moiety

in Co$_1$-N/P-C, thus demonstrating its versatile catalytic efficiencies and great potential for practical applications.

Considering the gas-liquid-solid three-phase reaction system, adsorption and diffusion of nitroarene play pivotal roles in determining the catalytic efficiency [28]. Hence, adsorption experiments of

nitroarene were performed to unveil the excellent catalytic characteristics of Co$_1$-N/P-C. As shown in Fig. S24, the absorption peak of *p*-CNB at about 280 nm dramatically decreases in intensity after exposure to Co$_1$-N/P-C and Co$_1$-N-C. Quantitative analysis reveals that Co$_1$-N/P-C exhibits a superior adsorption capacity (596 μmol g^{-1}) than that of Co$_1$-N-C (518 μmol g^{-1}), indicating the extraordinary affinity of Co-N$_2$P$_2$ toward *p*-CNB. To further uncover the adsorption behavior of *p*-CNB, in-situ FT-IR measurements were conducted on Co$_1$-N-C and Co$_1$-N/P-C (Fig. 5a-b). In the presence of Co$_1$-N-C, two characteristic bands of ν_{as} (1509 cm^{-1}) and ν_s (1352 cm^{-1}) are observed, indicating chemisorption of —NO$_2$ groups on the surface of Co$_1$-N-C. For the Co$_1$-N/P-C sample, a slight red shift of the two bands (1507 and 1340 cm^{-1}) can be observed, implying enhanced adsorption of the nitro group [49]. Notably, the relative intensity of ν_s(NO$_2$) on Co$_1$-N/P-C is significantly amplified compared to that of Co$_1$-N-C, which can be ascribed to the cleavage of N–O bond in —NO$_2$ to generate the nitroso intermediates. The aforementioned results confirm that the moderately electron-enriched Co center of the Co-N$_2$P$_2$ configuration can effectively facilitate the polarization and dissociation of nitro group. Moreover, given that the hydrogenation of *p*-CNB is also constrained by the adsorption and activation of hydrogen species, the interaction with H$_2$ was investigated by H$_2$-TPD technique. As displayed in Fig. 5c, the H$_2$ desorption peak primarily occurs at 535 K over Co$_1$-N-C, whereas Co$_1$-N/P-C presents an additional prominent peak at around 697 K, indicating its much stronger adsorption interaction with H$_2$. These experimental results strongly support the conclusion drawn from the above DFT predictions, which signifies that the incorporation of moderate P atoms can efficiently reinforce the adsorption and activation of the nitroarene and H$_2$ substrates, thereby guaranteeing the smooth transformation of nitroarene into corresponding aromatic amines.

Targeted DFT calculations were further conducted to gain a more comprehensive understanding of the prominent catalytic efficiency of Co-N$_2$P$_2$ configuration. Generally, the hydrogenation of nitroarenes involves adsorption and activation of H$_2$ and nitroarenes at the active sites. Therefore, the properties of H$_2$ adsorption-activation at single-atom sites as well as electronic interactions were first probed. As shown in Fig. S25, the adsorption of H$_2$ over the two structures indicates that Co-N$_2$P$_2$ harvests a greater bond length of H-H compared to that of Co-N$_4$, indicating its enhanced ability for H$_2$ activation. Upon activation by the active site, one of the H atoms attaches to the Co center (Lewis acid), assuming an electronegative disposition to form Co-H$^{\delta-}$. While the other H atom transfers to the neighboring N atom (Lewis base) for Co-N$_4$, resulting in the formation of N-H$^{\delta+}$. Conversely, in terms of Co-N$_2$P$_2$, the H$^{\delta+}$ atom is more favorable to attach to the coordinated P atom, which results in a shorter Co-H bond length and larger Bader charge transfer number (0.39 vs 0.096) from Co to H$^{\delta-}$. The intensified heterolytic dissociation of H$_2$ is conducive to the selective hydrogenation of the polar nitro group in nitroarenes. Moreover, the H$_2$ dissociation on the Co-N$_2$P$_2$ surface is exothermic (−0.1 eV) with an energy barrier of 0.71 eV, but endothermic (1.14 eV) with an increased energy barrier of 2.06 eV for the Co-N$_4$ motif (Fig. 5d). Subsequently, the reaction pathways over the catalysts involved in the hydrogenation of *p*-CNB to *p*-chloroaniline were investigated, namely, PhNO$_2$ * → PhNOOH* → PhNO* → PhNOH* → PhNHOH* → PhNH* → PhNH$_2$ * (Fig. S26). Remarkably, compared with traditional Co-N$_4$ configuration, Co-N$_2$P$_2$ exhibits stronger binding interactions with the reaction intermediates (Fig. S27) and much lower Gibbs free energy barriers (Fig. 5e) during the hydrogenation processes, revealing the accelerated reaction kinetics. Therefore, by incorporating two coordinated P atoms to precisely manipulate the local coordination environment, the Co$_1$-N/P-C catalyst with favorable Co-N$_2$P$_2$ coordination achieves reinforced heterolytic dissociation of H$_2$ and accelerated reaction kinetics, thus significantly boosting the catalytic selective hydrogenation of nitroarenes.

4. Conclusion

In conclusion, guided by DFT theoretical predictions, a novel Co-based single-atom catalyst featuring Co-N$_2$P$_2$ configuration has been delicately designed and successfully synthesized through a sacrificial template strategy. The local coordination of atomic Co centers can be
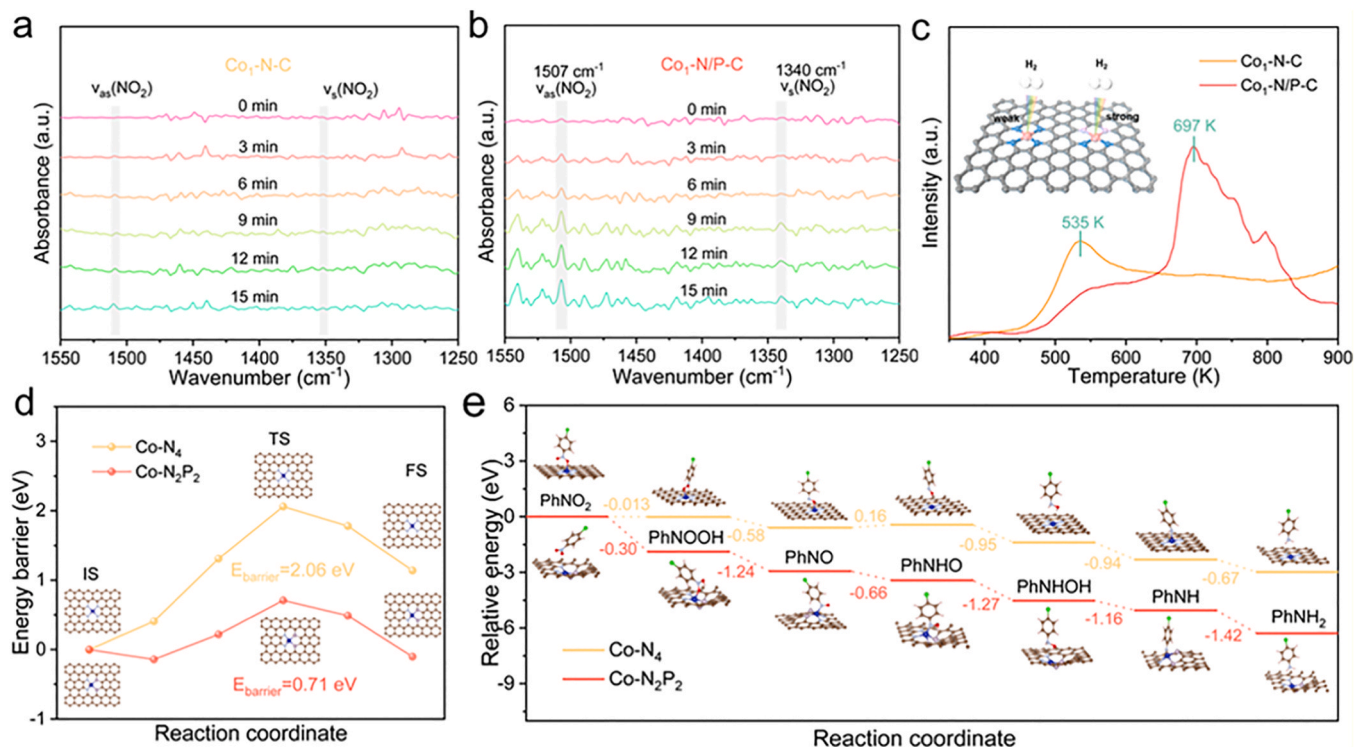

Fig. 5. (a) *In-situ* FT-IR spectra of *p*-CNB adsorbed on (a) Co$_1$-N-C and (b) Co$_1$-N/P-C, respectively. (c) H$_2$-TPD tests of Co$_1$-N-C and Co$_1$-N/P-C. (d) Energy barriers of H$_2$ dissociation on Co$_1$-N-C and Co$_1$-N/P-C. (e) Potential energy profiles of *p*-NCB hydrogenation on Co$_1$-N-C and Co$_1$-N/P-C.

effectively manipulated by adjusting the number of coordinated P atoms, resulting in distinct catalytic properties. Among the various Co-$N_xP_{(4-x)}$ models, the Co-N_2P_2 configuration exhibits a desirable chemical affinity toward nitroarene and H_2, promoted heterolytic dissociation of H_2, and accelerated reaction kinetics. Consequently, the prepared Co$_1$-N/P-C catalyst exhibits distinguished catalytic activity (overall TOF of 241.5 h^{-1}) and selectivity (>99%), as well as exceptional stability for the selective hydrogenation of various functionalized nitroarenes, surpassing other coordination configurations and most reported non-precious metal catalysts. This work not only presents a feasible strategy for the precise synthesis of advanced single-atom catalysts for selective hydrogenation of nitroarenes but also deepens our understanding of the relationship between coordination structure and catalytic performance for chemical transformations.

CRediT authorship contribution statement

Kong Debin: Writing – review & editing, Validation, Supervision, Funding acquisition. **Xue Song:** Writing – review & editing, Methodology. **Li Yanpeng:** Validation, Software, Data curation. **Zhao Qingshan:** Writing – review & editing, Validation, Supervision, Resources, Methodology, Investigation, Conceptualization. **Wang Libo:** Methodology, Data curation. **Cao Fengliang:** Writing – original draft, Investigation, Formal analysis, Data curation, Conceptualization. **Ni Wanxin:** Formal analysis, Data curation. **Wu Mingbo:** Validation, Supervision, Resources, Project administration. **Zhi Linjie:** Writing – review & editing, Validation, Supervision, Resources, Funding acquisition.

Declaration of Competing Interest

The authors declare that they have no known competing financial interests or personal relationships that could have appeared to influence the work reported in this paper.

Data Availability

The data that has been used is confidential.

Acknowledgments

Appendix A. Supporting information

Supplementary data associated with this article can be found in the online version at doi:10.1016/j.apcatb.2024.123762.

References

[1] R. Jagadeesh, A. Surkus, H. Junge, M. Pohl, J. Radnik, J. Rabeah, H. Huan, V. Schünemann, A. Brückner, M. Beller, Nanoscale Fe$_2$O$_3$-based catalysts for selective hydrogenation of nitroarenes to anilines, Science 342 (2013) 1073–1076.

[2] L. Zhang, M. Zhou, A. Wang, T. Zhang, Selective hydrogenation over supported metal catalysts: from nanoparticles to single atoms, Chem. Rev. 120 (2) (2020) 683–733.

[3] H. Wei, X. Liu, A. Wang, L. Zhang, B. Qiao, X. Yang, Y. Huang, S. Miao, J. Liu, T. Zhang, FeO$_x$-supported platinum single-atom and pseudo-single-atom catalysts for chemoselective hydrogenation of functionalized nitroarenes, Nat. Commun. 5 (2014) 5634.

[4] D. Formenti, F. Ferretti, F.K. Scharnagl, M. Beller, Reduction of nitro compounds using 3d-non-noble metal catalysts, Chem. Rev. 119 (4) (2019) 2611–2680.

[5] W. Liu, H. Feng, Y. Yang, Y. Niu, L. Wang, P. Yin, S. Hong, B. Zhang, X. Zhang, M. Wei, Highly-efficient RuNi single-atom alloy catalysts toward chemoselective hydrogenation of nitroarenes, Nat. Commun. 13 (2022) 3188.

[6] H. Yan, X. Zhao, N. Guo, Z. Lyu, Y. Du, S. Xi, R. Guo, C. Chen, Z. Chen, W. Liu, C. Yao, J. Li, S.J. Pennycook, W. Chen, C. Su, C. Zhang, J. Lu, Atomic engineering of high-density isolated Co atoms on graphene with proximal-atom controlled reaction selectivity, Nat. Commun. 9 (2018) 3197.

[7] S. Tian, B. Wang, W. Gong, Z. He, Q. Xu, W. Chen, Q. Zhang, Y. Zhu, J. Yang, Q. Fu, C. Chen, Y. Bu, L. Gu, X. Sun, H. Zhao, D. Wang, Y. Li, Dual-atom Pt heterogeneous catalyst with excellent catalytic performances for the selective hydrogenation and epoxidation, Nat. Commun. 12 (2021) 3181.

[8] A. Han, J. Zhang, W. Sun, W. Chen, S. Zhang, Y. Han, Q. Feng, L. Zheng, L. Gu, C. Chen, Q. Peng, D. Wang, Y. Li, Isolating contiguous Pt atoms and forming Pt-Zn intermetallic nanoparticles to regulate selectivity in 4-nitrophenylacetylene hydrogenation, Nat. Commun. 10 (2019) 3787.

[9] Q. Zhang, D. Xu, A. Cai, X. Hu, X. Li, W. Peng, Y. Li, F. Zhang, X. Fan, Chemoselective hydrogenation of nitro compounds by MoS$_2$ via introduction of independent active hydrogen-donating sites, ACS Catal. 12 (19) (2022) 12170–12178.

[10] P. Zhou, L. Jiang, F. Wang, K. Deng, K. Lv, Z. Zhang, High performance of a cobalt–nitrogen complex for the reduction and reductive coupling of nitro compounds into amines and their derivatives, Sci. Adv. 3 (2017) e1601945.

[11] J. Fu, J. Dong, R. Si, K. Sun, J. Zhang, M. Li, N. Yu, B. Zhang, M.G. Humphrey, Q. Fu, J. Huang, Synergistic effects for enhanced catalysis in a dual single-atom catalyst, ACS Catal. 11 (4) (2021) 1952–1961.

[12] L. Liu, D.M. Meira, R. Arenal, P. Concepcion, A.V. Puga, A. Corma, Determination of the evolution of heterogeneous single metal atoms and nanoclusters under reaction conditions: which are the working catalytic sites? ACS Catal. 9 (12) (2019) 10626–10639.

[13] N. Yang, H. Cheng, X. Liu, Q. Yun, Y. Chen, B. Li, B. Chen, Z. Zhang, X. Chen, Q. Lu, J. Huang, Y. Huang, Y. Zong, Y. Yang, L. Gu, H. Zhang, Amorphous/crystalline hetero-phase Pd nanosheets: one-pot synthesis and highly selective hydrogenation reaction, Adv. Mater. 30 (39) (2018) e1803234.

[14] Y. Zhong, P. Liao, J. Kang, Q. Liu, S. Wang, S. Li, X. Liu, G. Li, Locking effect in Metal@MOF with superior stability for highly chemoselective catalysis, J. Am. Chem. Soc. 145 (8) (2023) 4659–4666.

[15] L. Wang, C. Zhu, M. Xu, C. Zhao, J. Gu, L. Cao, X. Zhang, Z. Sun, S. Wei, W. Zhou, W.X. Li, J. Lu, Boosting activity and stability of metal single-atom catalysts via regulation of coordination number and local composition, J. Am. Chem. Soc. 143 (45) (2021) 18854–18858.

[16] C. Wang, S. Mao, Z. Wang, Y. Chen, W. Yuan, Y. Ou, H. Zhang, Y. Gong, Y. Wang, B. Mei, Z. Jiang, Y. Wang, Insight into single-atom-induced unconventional size dependence over CeO$_2$-supported Pt catalysts, Chem 6 (3) (2020) 752–765.

[17] Z. Li, M. Zhang, X. Dong, S. Ji, L. Zhang, L. Leng, H. Li, J. Horton, Q. Xu, J. Zhu, Strong electronic interaction of indium oxide with palladium single atoms induced by quenching toward enhanced hydrogenation of nitrobenzene, Appl. Catal. B Environ. 313 (2022) 121462.

[18] C. Chen, W. Ou, K. Yam, S. Xi, X. Zhao, S. Chen, J. Li, P. Lyu, L. Ma, Y. Du, W. Yu, H. Fang, C. Yao, X. Hai, H. Xu, M.J. Koh, S.J. Pennycook, J. Lu, M. Lin, C. Su, C. Zhang, J. Lu, Zero-valent palladium single-atoms catalysts confined in black phosphorus for efficient semi-hydrogenation, Adv. Mater. 33 (2021) 2008471.

[19] T. Schwob, R. Kempe, A. Reusable, Co catalyst for the selective hydrogenation of functionalized nitroarenes and the direct synthesis of imines and benzimidazoles from nitroarenes and aldehydes, Angew. Chem. Int. Ed. 55 (48) (2016) 15175–15179.

[20] H. Yan, C.L. Su, J. He, W. Chen, Single-atom catalysts and their applications in organic chemistry, J. Mater. Chem. A 6 (19) (2018) 8793–8814.

[21] J. Liu, Z. Jin, X. Wang, J. Ge, C. Liu, M. Xing, Recent advances in active sites identification and regulation of M-N/C electro-catalysts towards ORR, Sci. China Chem. 62 (6) (2019) 669–683.

[22] S. Jun, S. Choi, J. Kim, S. Kwon, S. Park, H. Jang, Non-noble metal single atom catalysts for electrochemical energy coversion reactions, Chin. J. Catal. 50 (2023) 195–214.

[23] X. Long, Z. Li, G. Gao, P. Sun, J. Wang, B. Zhang, J. Zhong, Z. Jiang, F. Li, Graphitic phosphorus coordinated single Fe atoms for hydrogenative transformations, Nat. Commun. 11 (2020) 4074.

[24] M. Li, C. Zhang, Y. Tang, Q. Chen, W. Li, Z. Han, S. Chen, C. Lv, Y. Yan, Y. Zhang, W. Zheng, P. Wang, X. Guo, W. Ding, Environment molecules boost the chemoselective hydrogenation of nitroarenes on cobalt single-atom catalysts, ACS Catal. 12 (19) (2022) 11960–11973.

[25] X. Hai, X. Zhao, N. Guo, C. Yao, C. Chen, W. Liu, Y. Du, H. Yan, J. Li, Z. Chen, X. Li, Z. Li, H. Xu, P. Lyu, J. Zhang, M. Lin, C. Su, S. Pennycook, C. Zhang, S. Xi, J. Lu, Engineering local and global structures of single Co atoms for a superior oxygen reduction reaction, ACS Catal. 10 (2020) 5862–5870.

[26] D. Zhou, X. Zhang, X. Liu, H. Qi, Q. Liu, J. Yang, Y. Su, J. Ma, J. Yin, A. Wang, Tuning the coordination environment of single-atom catalyst M-N-C towards selective hydrogenation of functionalized nitroarenes, Nano Res. 15 (1) (2021) 519–527.

[27] J. He, N. Li, Z. Li, M. Zhong, Z.X. Fu, M. Liu, J.C. Yin, Z. Shen, W. Li, J. Zhang, Z. Chang, X. Bu, Strategic defect engineering of metal-organic frameworks for

optimizing the fabrication of single-atom catalysts, Adv. Funct. Mater. 31 (2021) 2103597.

[28] L. Zhu, Y. Sun, H. Zhu, G. Chai, Z. Yang, C. Shang, H. Ye, B. Chen, A. Kroner, Z. Guo, Effective ensemble of Pt single atoms and clusters over the (Ni,Co)(OH)$_2$ substrate catalyzes highly selective, efficient, and stable hydrogenation reactions, ACS Catal. 12 (13) (2022) 8104–8115.

[29] J. Wan, Z. Zhao, H. Shang, B. Peng, W. Chen, J. Pei, L. Zheng, J. Dong, R. Cao, R. Sarangi, Z. Jiang, D. Zhou, Z. Zhuang, J. Zhang, D. Wang, Y. Li, In situ phosphatizing of triphenylphosphine encapsulated within metal-organic frameworks to design atomic Co$_1$-P$_1$N$_3$ interfacial structure for promoting catalytic performance, J. Am. Chem. Soc. 142 (18) (2020) 8431–8439.

[30] Y. Chen, R. Gao, S. Ji, H. Li, K. Tang, P. Jiang, H. Hu, Z. Zhang, H. Hao, Q. Qu, X. Liang, W. Chen, J. Dong, D. Wang, Y. Li, Atomic-Level modulation of electronic density at cobalt single-atom sites derived from metal-organic frameworks: enhanced oxygen reduction performance, Angew. Chem. Int. Ed. 60 (6) (2021) 3212–3221.

[31] F. Lu, K. Fan, L. Cui, B. Li, Y. Yang, L. Zong, L. Wang, Engineering FeN$_4$ active sites onto nitrogen-rich carbon with tubular channels for enhanced oxygen reduction reaction performance, Appl. Catal. B: Environ. 313 (2022) 121464.

[32] X. Hai, S. Xi, S. Mitchell, K. Harrath, H. Xu, D.F. Akl, D. Kong, J. Li, Z. Li, T. Sun, H. Yang, Y. Cui, C. Su, X. Zhao, J. Li, J. Perez-Ramirez, J. Lu, Scalable two-step annealing method for preparing ultra-high-density single-atom catalyst libraries, Nat. Nanotechnol. 17 (2022) 174–181.

[33] S. Shah, T. Najam, J. Yang, M. Javed, L. Peng, Z. Wei, Modulating the microenvironment structure of single Zn atom: ZnN$_4$P/C active site for boosted oxygen reduction reaction. Chinese, J. Catal. 43 (2022) 2193–2201.

[34] T. Sun, S. Mitchell, J. Li, P. Lyu, X. Wu, J. Pérez-Ramírez, J. Lu, Design of local atomic environments in single-atom electrocatalysts for renewable energy conversions, Adv. Mater. 33 (2021) 2003075.

[35] X. Hai, Y. Zheng, Q. Yu, N. Guo, S. Xi, X. Zhao, S. Mitchell, X. Luo, V. Tulus, M. Wang, X. Sheng, L. Ren, X. Long, J. Li, P. He, H. Lin, Y. Cui, X. Peng, J. Shi, J. Wu, C. Zhang, R. Zou, G. Guillén-Gosálbez, J. Pérez-Ramírez, M.J. Koh, Y. Zhu, J. Li, J. Lu, Geminal-atom catalysis for cross-coupling, Nature 622 (7984) (2023) 754–760.

[36] X. Wu, H. Zhang, S. Zuo, J. Dong, Y. Li, J. Zhang, Y. Han, Engineering the coordination sphere of isolated active sites to explore the intrinsic activity in single-atom catalysts, Nano-Micro Lett. 13 (2021) 136.

[37] G. Zhang, F. Tang, X. Wang, L. Wang, Y.-N. Liu, Atomically dispersed Co–S–N active sites anchored on hierarchically porous carbon for efficient catalytic hydrogenation of nitro compounds, ACS Catal. 12 (10) (2022) 5786–5794.

[38] H. Jin, P. Li, P. Cui, J. Shi, W. Zhou, X. Yu, W. Song, C. Cao, Unprecedentedly high activity and selectivity for hydrogenation of nitroarenes with single atomic Co$_1$-N$_3$P$_1$ sites, Nat. Commun. 13 (2022) 723.

[39] X. Wang, X. Zhou, C. Li, H. Yao, C. Zhang, J. Zhou, R. Xu, L. Chu, H. Wang, M. Gu, H. Jiang, M. Huang, Asymmetric Co–N$_3$P$_1$ trifunctional catalyst with tailored electronic structures enabling boosted activities and corrosion resistance in an uninterrupted seawater splitting system, Adv. Mater. 34 (2022) 2204021.

[40] M. Monai, A. Banerjee, Catalyst-support interactions in heterogeneous catalysis: from fundamental concepts to applications, Catal. Today 382 (2021) 1–2.

[41] S. Hu, W.-X. Li, Sabatier principle of metal-support interaction for design of ultrastable metal nanocatalysts, Science 374 (2021) 1360–1365.

[42] X. Sun, Y. Tuo, C. Ye, C. Chen, Q. Lu, G. Li, P. Jiang, S. Chen, P. Zhu, M. Ma, J. Zhang, J.H. Bitter, D. Wang, Y. Li, Phosphorus induced electron localization of single iron sites for boosted CO$_2$ electroreduction reaction, Angew. Chem. Int. Ed. 60 (44) (2021) 23614–23618.

[43] S. An, G. Zhang, T. Wang, W. Zhang, K. Li, C. Song, J.T. Miller, S. Miao, J. Wang, X. Guo, High-density ultra-small clusters and single-atom Fe sites embedded in graphitic carbon nitride (g-C$_3$N$_4$) for highly efficient catalytic advanced oxidation processes, ACS Nano 12 (9) (2018) 9441–9450.

[44] Q. Zhao, W. Ni, X. Tan, F. Cao, T. Liu, H. Huang, Z. Cheng, Y. Li, S. He, H. Ning, M. Wu, A "Trojan horse" strategy towards robust Co-N$_4$ active sites accommodated in micropore defect-rich carbon nanosheets for boosting selective hydrogenation of nitroarenes, J. Mater. Chem. A 10 (2022) 9435–9444.

[45] F. Cao, Q. Zhao, D. Kong, X. Tan, X. Li, T. Liu, L. Zhi, M. Wu, Turning the coordination environment of atomic Fe-N$_4$ center by peripheral nitrogen species for boosted catalytic performance, Chem. Eng. J. 473 (2023) 145181.

[46] F. Cao, Q. Zhao, D. Kong, X. Tan, X. Li, T. Liu, L. Zhi, M. Wu, Dual-active-sites design of Co@C catalysts for ultrahigh selective hydrogenation of N-heteroarenes, Chem 6 (11) (2020) 2994–3006.

[47] M. Zhang, H. Li, J. Chen, F.-X. Ma, L. Zhen, Z. Wen, C.-Y. Xu, High-loading Co single atoms and clusters active sites toward enhanced electrocatalysis of oxygen reduction reaction for high-performance Zn-air battery, Adv. Funct. Mater. (2022) 2209726.

[48] K. Liu, X. Wang, S. Gu, H. Yuan, F. Jiang, Y. Li, W. Tan, Q. Long, J. Chen, Z. Xu, Z. Lu, N, S-coordinated Co single atomic catalyst boosting adsorption and conversion of lithium polysulfides for lithium-sulfur batteries, Small 18 (2022) 2204707.

[49] M.L. Gao, L. Li, Z.X. Sun, J.R. Li, H.L. Jiang, Facet engineering of a metal–organic framework support modulates the microenvironment of palladium nanoparticles for selective hydrogenation, Angew. Chem. Int. Ed. 61 (2022) e202211216.